ISSN 1330–0016
CODEN FIZBE7

COULOMB GAUGE HAMILTONIAN: ADVANCES AND APPLICATIONS

STEPHEN R. COTANCH

Department of Physics, North Carolina State University, Raleigh, NC 27695-8202, USA
E-mail address: cotanch@ncsu.edu

Received 19 August 2003; Accepted 26 April 2004
Online 16 July 2004

Theoretical developments and applications of an effective QCD Hamiltonian in the Coulomb gauge are summarized. BCS, TDA and RPA many-body diagonalizations in the quark and gluon sectors are reported for meson and glueball spectra, respectively. The model glueball Regge trajectories are in good agreement with the established pomeron and a recently observed odd signature daughter. Using the pomeron-glueball connection and vector meson dominance, glueball photoproduction cross sections and decays are calculated and a glueball experimental signature is predicted. The pseudoscalar-vector meson mass splittings are also investigated using a hyperfine interaction based upon transverse gluon exchange. An improved meson spectrum is obtained and the dominant role of chiral symmetry in the π-ρ mass difference is confirmed.

PACS numbers: 11.30.Rd, 12.38.Lg, 12.39.Mk, 12.40.Vv, 12.40.Yx UDC 539.12.1
Keywords: QCD, Coulomb gauge Hamiltonian, hyperfine interaction, chiral symmetry, glueballs, pomeron

1. Introduction

The non-Abelian, non-perturbative nature of QCD bound states has challenged realistic numerical hadronic investigations for several decades. However, with more powerful computational resources and improved theoretical formulations significant progress has been achieved in understanding hadronic structure. In particular both lattice simulations and effective Hamiltonian diagonalizations utilizing many-body techniques have provided important insight regarding the structure of mesons [1, 2], exotics glueballs [3, 4] and hybrid hadron [5] systems.

This paper summarizes recent highlights of a many-body effective Hamiltonian approach. In the next few sections the Hamiltonian is discussed along with the equations of motion: Bardin-Cooper-Schrieffer [BCS] gap equations for the vacuum, Tamm-Dancoff [TDA] and random phase approximation [RPA] for the hadron

masses (excited states). In section 3, the low-lying model glueball states are compared to lattice and the similarity to the pomeron is detailed including a recently discovered odd signature daughter pomeron observed in deep inelastic scattering [6]. This section also contains glueball photoproduction cross section predictions and decay widths. Section 4 provides numerical results utilizing a transverse effective hyperfine interaction and a longitudinal confining potential that was determined self-consistently from the model vacuum. An improved description of the light and heavy meson spin splittings is obtained and the dominant contribution, almost 70%, from chiral symmetry to the π-ρ mass difference is verified in the presence of a realistic hyperfine interaction.

2. Effective QCD Hamiltonian

Suppressing the Fadeev-Popov determinant, the QCD Hamiltonian in the Coulomb gauge ($\nabla\cdot\mathbf{A}^a = 0$) with coupling constant g has the general structure

$$H_{eff} = \int \mathrm{d}\mathbf{x}\, \Psi^\dagger(\mathbf{x})\big[-\mathrm{i}\,\boldsymbol{\alpha}\cdot\boldsymbol{\nabla} + \beta\, m\big]\Psi(\mathbf{x}) - \frac{1}{2}\int \mathrm{d}\mathbf{x}\,\mathrm{d}\mathbf{y}\,\rho^a(\mathbf{x})V(\mathbf{x},\mathbf{y})\,\rho^a(\mathbf{y}) + \frac{1}{2}\int \mathrm{d}\mathbf{x}\,\big[\boldsymbol{\Pi}^a(\mathbf{x})\cdot\boldsymbol{\Pi}^a(\mathbf{x}) + \mathbf{B}^a(\mathbf{x})\cdot\mathbf{B}^a(\mathbf{x})\big] + g\int \mathrm{d}\mathbf{x}\,\mathbf{J}^a(\mathbf{x})\cdot\mathbf{A}^a(\mathbf{x})\,, \quad (1)$$

with current quark mass, m, field, Ψ, quark/gluon color charge density $\rho^a(\mathbf{x}) = \Psi^\dagger(\mathbf{x})T^a\Psi(\mathbf{x}) + f^{abc}\mathbf{A}^b(\mathbf{x})\cdot\boldsymbol{\Pi}^c(\mathbf{x})$, quark color current $\mathbf{J}^a = \Psi^\dagger\boldsymbol{\alpha}T^a\Psi$, gauge fields, $\mathbf{A}^a$, and conjugate momentum, $\boldsymbol{\Pi}^a = -\mathbf{E}^a$ (electric). The non-Abelian color magnetic field is $\mathbf{B}^a = \boldsymbol{\nabla}\times\mathbf{A}^a + \frac{1}{2}f^{abc}\mathbf{A}^b\times\mathbf{A}^c$.

The fields are expanded in normal modes (color vectors $\hat{\varepsilon}_c$, $\boldsymbol{\epsilon}^a_\lambda$, with indices

$$\Psi(\mathbf{x}) = \sum_{c\lambda}\int \frac{\mathrm{d}\mathbf{k}}{(2\pi)^3}\left[u_\lambda(\mathbf{k})b^c_\lambda(\mathbf{k}) + v_\lambda(-\mathbf{k})d^{c\dagger}_\lambda(-\mathbf{k})\right]\hat{\varepsilon}_c\,\mathrm{e}^{\mathrm{i}\,\mathbf{k}\cdot\mathbf{x}}\,, \quad (2)$$

$$\mathbf{A}^a(\mathbf{x}) = \int \frac{\mathrm{d}\mathbf{k}}{(2\pi)^3}\frac{1}{\sqrt{2\omega_k}}[\mathbf{a}^a(\mathbf{k}) + \mathbf{a}^{a\dagger}(-\mathbf{k})]\mathrm{e}^{\mathrm{i}\,\mathbf{k}\cdot\mathbf{x}}\,, \quad (3)$$

$$\boldsymbol{\Pi}^a(\mathbf{x}) = -\mathrm{i}\int \frac{\mathrm{d}\mathbf{k}}{(2\pi)^3}\sqrt{\frac{\omega_k}{2}}[\mathbf{a}^a(\mathbf{k}) - \mathbf{a}^{a\dagger}(-\mathbf{k})]\mathrm{e}^{\mathrm{i}\,\mathbf{k}\cdot\mathbf{x}}\,, \quad (4)$$

$c = 1,2,3$, $a = 1,2,\ldots 8$, $\mu = \pm 1/2$, $\lambda = \pm 1$) subject to the Coulomb gauge transverse condition, $\mathbf{k}\cdot\mathbf{a}^a(\mathbf{k}) = 0$, where $\mathbf{a}^a(\mathbf{k}) = \sum_\lambda \boldsymbol{\epsilon}^a_\lambda(\mathbf{k})a^a_\lambda(\mathbf{k})$.

3. Gluon gap equation and glueballs

In our gluon sector calculations, the color magnetic fields $\mathbf{B}^a$ are replaced by their Abelian components $\mathbf{B}^a_A = \nabla\times\mathbf{A}^a$ and only the gluon color charge density

is retained. The hyperfine interaction (last term in Eq. (1)) is also suppressed so there is no coupling to the quark sector (quenched approximation). Because the gluon coupling effect on the quark sector is significant, this interaction is included in our meson calculations described in the next section. The complicated confining interaction V is also replaced by a Cornell potential, $V(r) = |\mathbf{x}-\mathbf{y}|) = -\alpha_s/r + \sigma r$, with string tension, $\sigma = 0.135$ GeV^2, from lattice gauge calculations and $\alpha_s = 0.2$. A cut-off parameter, $\Lambda = 4$ GeV, is used to regularize the logarithmic divergence in the gap equation.

Next, the gluon Fock operators are dressed by a similarity transformation (BCS rotation) to a quasiparticle basis $\alpha^a_\lambda(\mathbf{k}) = \cosh\Theta_k\, a^a_\lambda(\mathbf{k}) + \sinh\Theta_k\, a^{a\dagger}_\lambda(-\mathbf{k})$, where $\Theta_k = \Theta(k)$, is the BCS angle. Then, the Hamiltonian is diagonalized variationally, $\delta\langle\Omega|H_{\rm eff} - E|\Omega\rangle = 0$, for the ground state (vacuum), $|\Omega\rangle$, with the gluon self-energy, given by $\omega_k = k\mathrm{e}^{-2\Theta_k}$, the variational parameter. This generates an improved BCS vacuum with correlated Cooper pairs (gluon condensates). The variation yields the nonlinear gluon mass gap equation

$$\omega_k^2 = k^2 - \frac{3}{4}\int \frac{\mathrm{d}\mathbf{q}}{(2\pi)^3} V(|\mathbf{k}-\mathbf{q}|)(1+(\hat{\mathbf{k}}\cdot\hat{\mathbf{q}})^2)\left(\frac{w_q^2 - w_k^2}{w_q}\right). \tag{5}$$

The non-zero quasiparticle constituent mass can be extracted from the gluon self-energy at low momentum and is about 800 MeV. The gap angle also determines the gluon condensate, $\langle\alpha_s G^a_{\mu\nu}G^{\mu\nu}_a\rangle = (433\ \mathrm{MeV})^4$, which has been regularized and is in good agreement with the QCD sum rule result $(441\ \mathrm{MeV})^4$.

The TDA glueball wavefunction for two constituent gluons is given by

$$|\Psi^{JPC}_{LS}\rangle = \sum_{a\lambda_1\lambda_2}\int \frac{\mathrm{d}\mathbf{k}}{(2\pi)^3}\Phi^{JPC}_{LS\lambda_1\lambda_2}(\mathbf{k})\alpha^{a\dagger}_{\lambda_1}(\mathbf{k})\alpha^{a\dagger}_{\lambda_2}(-\mathbf{k})|\Omega\rangle\,. \tag{6}$$

Here $\mathbf{J} = \mathbf{L} + \mathbf{S}$ is the total angular momentum, P is the parity, C is the C-parity, L is the orbital anglular momentum and $S = 0, 1$ or 2 is the total intrinsic gluon spin. Using this quasiparticle basis, the excited glueball spectrum was computed by diagonalizing the above specified Hamiltonian in the TDA truncated at the 1p-1h quasiparticle level. See Refs. [3] and [4] for further details. The TDA $J^{PC} = 0^{++}, 2^{++}$ and 3^{++} states are plotted in Fig. 1 along with lattice gauge measurements (horizontal lines) [7] for states up to $J^{PC} = 4^{++}$. The lattice errors are large, but notice the proximity of the theoretical states to the pomeron and recently discovered [6] odd signature daughter pomeron having trajectories given by $\alpha(t) = bt + \alpha(0)$, with $b \approx 0.25$ GeV^{-2} and intercepts 1.08 and .88, respectively. Related, a new lattice study reports [8] a 6^{++} glueball (not shown) which is also close to the conventional pomeron. The 0^{++} ($L = S = 0$) glueball (dark circle) is precluded by definition from both pomerons and lies on an even signature but lower daughter trajectory (dashed line). The slopes of all (not shown) TDA trajectories are the same and as represented by the $S = 0$ glueball predictions (dark circles for $J = L = 0$, 2 and 4).

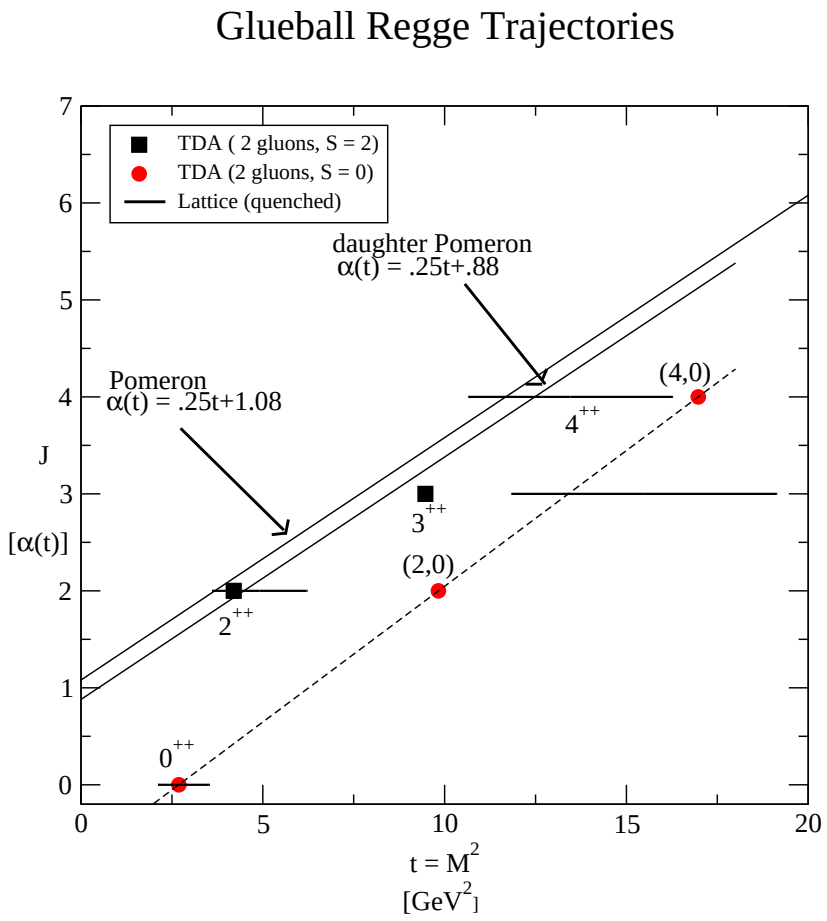

Fig. 1. Even and odd signature pomerons (solid lines) compared to the TDA (boxes and dark circles) and lattice (horizontal lines) glueball states.

The glueball-pomeron connection permits glueball photoproduction predictions by simply substituting phenomenological pomeron-hadron couplings for the required glueball-hadron vertex constants. Invoking vector meson dominance [VMD] and universality for the vector meson-glueball couplings (gluons are flavor blind), the exclusive cross section for $\mathrm{p}(\gamma, G \to VV)\mathrm{p}$ was computed and is displayed in Fig. 2 versus the invariant mass for the two decaying vector mesons. Both ρ and ω t channel exchange along with s and u channel proton Born terms are included. Contrast the cross section enhancement for glueball formation and decay to $\rho\rho$ and $\omega\omega$ with the lower curve for two vector meson production without glueball formation. The remaining curve at higher invariant mass represents $\phi\phi$ photoproduction which has a threshold above the 0^{++} glueball state. Because of the dominant $\rho \to \pi\pi$ and $\omega \to \pi\pi\pi$ decays, a distinctive glueball signature emerges as an enhanced four and

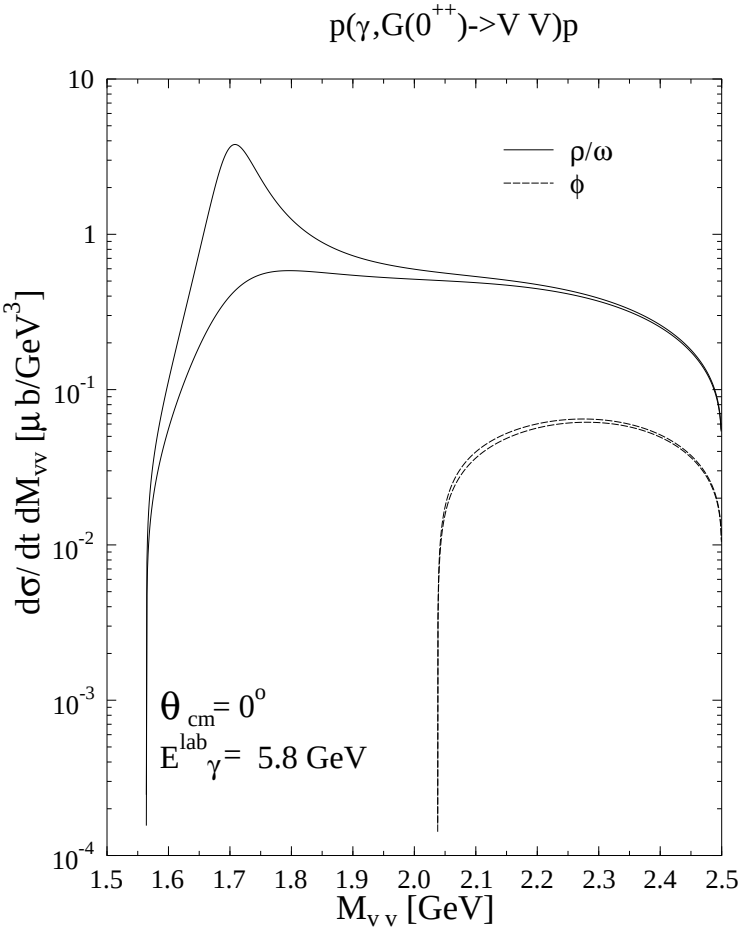

Fig. 2. Glueball photoproduction and decay to two vector mesons.

six pion correlation observed in the 1.7 GeV region. Related, if the glueball mass is slighter larger, which may shift due to mixing with scalar mesons, the $\omega\phi$ decay channel might be open which would lead to a novel $\pi^+\pi^0\pi^-\mathrm{K}\bar{\mathrm{K}}$ decay.

Finally, from VMD the decay widths for several two-body channels have been computed. The vector meson and radiative decay rates are: $\rho\rho$, 133.2 MeV; $\omega\omega$, 34.6 MeV; $\rho\gamma$, 0.866 keV; $\omega\gamma$, 0.844 keV; $\phi\gamma$, 0.454 keV; $\gamma\gamma$, 2.6 keV.

4. Quark gap equation and mesons

For the quark sector, the hyperfine interaction is now included. Only a synopsis is provided here but a more complete discussion can be found elsewhere [9]. The explicit gluon degrees of freedom can be removed from the hyperfine Hamiltonian term by P, Q projections or similarity transformations. The resulting effective quark

hyperfine interaction has the general transverse vector-vector form

$$H_T = \int \mathrm{d}\mathbf{x}\,\mathrm{d}\mathbf{y}\, J_i^a(\mathbf{x}) U_{ij}(\mathbf{x},\mathbf{y}) J_j^a(\mathbf{y})\,, \tag{7}$$

where U_{ij} is a complicated, but non-confining, kernel. In the simplest approximation of one gluon exchange, $U_{ij} \to \delta_{ij}\alpha_s/|\mathbf{x}-\mathbf{y}|$, where $\alpha_s = g^2/4\pi$. Consistency requires implementing the Coulomb gauge constraint and the specific transverse hyperfine interaction used in this work is

$$H_T = \frac{1}{2}\int \mathrm{d}\mathbf{x}\,\mathrm{d}\mathbf{y}\, J_i^a(\mathbf{x}) J_j^a(\mathbf{y}) \left(\delta_{ij} - \frac{\nabla_i \nabla_j}{\nabla^2}\right)_{\mathbf{x}} U(|\mathbf{x}-\mathbf{y}|)\ . \tag{8}$$

The hyperfine potential U and confining interaction V specifies the quark Hamiltonian. Instead of adopting the simple linear and Coulomb potentials used previously [1, 2], an improved confining interaction is now incorporated that was developed in Ref. [10]. That work determined both the quasiparticle basis and confining interaction self-consistently and reproduced lattice gauge simulations. This resulting interaction, which is similar to the Cornell potential, is more fundamentaly connected to the QCD model vacuum and can be accurately represented by the analytic form

$$\begin{aligned} V(p) &= C(p) \equiv -\frac{8.07}{p^2}\,\frac{\log^{-0.62}\left(p^2/m_g^2 + 0.82\right)}{\log^{0.8}\left(p^2/m_g^2 + 1.41\right)} \quad \text{for} \quad p > m_g\,, \\ V(p) &= L(p) \equiv -\frac{12.25\, m_g^{1.93}}{p^{3.93}} \quad \text{for} \quad p < m_g\,. \end{aligned} \tag{9}$$

The free parameter, m_g, sets the scale and is equivalent to a string tension.

The hyperfine potential is phenomenological and to study model sensitivity, four different interactions were used. Model 1 is a square well

$$\begin{aligned} U_1(p) &= 0 \quad \text{for} \quad p > \Lambda\,, \\ U_1(p) &= -U_h \quad \text{for} \quad p < \Lambda\,, \end{aligned} \tag{10}$$

with strength, U_h, and range, Λ. Model 2 reflects a massless transverse gluon exchange and is a Coulomb-like potential

$$\begin{aligned} U_2(p) &= C(p) \quad \text{for} \quad p > m_g\,, \\ U_2(p) &= -\frac{C_h}{p^2} \quad \text{for} \quad p < m_g\,. \end{aligned} \tag{11}$$

Model 3 entails a modified Coulomb/square well potential having a UV Coulomb tail matched to a constant in the IR

$$\begin{aligned} U_3(p) &= C(p) \quad \text{for} \quad p > m_g\,, \\ U_3(p) &= -C_h \quad \text{for} \quad p < m_g\,. \end{aligned} \tag{12}$$

Lastly, model 4 is a Yukawa-type potential corresponding to the exchange of a constituent gluon with mass m_g

$$\begin{aligned} U_4(p) &= C(p) \quad \text{for} \quad p > m_g\,, \\ U_4(p) &= -\frac{C_h}{p^2+m_g^2} \quad \text{for} \quad p < m_g\,. \end{aligned} \tag{13}$$

The potential $C(p)$ for the last three models is the same as in Eq. (9). The constant C_h was determined by matching the UV and IR regions at the transition scale m_g and there was no qualitative sensitivity to this scale.

The quark gap equation is determined the same way as in the gluon sector and constituent quarks are generated by dressing the current quarks through the quasiparticle transformation $B^c_\mu(\mathbf{k}) = \cos(\theta_k/2)\, b^c_\mu(\mathbf{k}) - \mu \sin(\theta_k/2), d^{c\dagger}_\mu(-\mathbf{k})$ and $D^c_\mu(-\mathbf{k}) = \cos(\theta_k/2)\, d^c_\mu(-\mathbf{k}) + \mu \sin(\theta_k/2)\, b^{c\dagger}_\mu(\mathbf{k})$. The quark gap angle, ϕ_k, is connected to the BCS angle, θ_k, by $\tan(\phi_k - \theta_k) = m/k$. The running constituent quark mass, M_k, is related to the gap angle by $M_k = E_k \sin\phi_k$, with $E_k = \sqrt{M_k^2 + k^2}$. The BCS quark condensate, $\langle \overline{q}q\rangle \equiv \langle \Omega|\overline{\Psi}(0)\Psi(0)|\Omega\rangle = -(3/\pi^2)\int k^2 \sin\phi_k \,\mathrm{d}k$, diverges quadratically for non-zero current quark mass and is regulated, $\langle \overline{q}q\rangle_{\rm reg} = -(3/\pi^2)\int k^2 \left(\sin\phi_k - \frac{m}{E_k}\right)\,\mathrm{d}k$, by subtracting the trivial condensate.

Performing the BCS vacuum variation generates the quark gap equation

$$\begin{aligned} k\, s_k - m_q\, c_k = \frac{2}{3}\int \frac{\mathrm{d}\mathbf{q}}{(2\pi)^3}\, [V(|\mathbf{k}-\mathbf{q}|)(s_k c_q x - s_q c_k) \\ -4(c_k s_q U(|\mathbf{k}-\mathbf{q}|) - c_q s_k W(|\mathbf{k}-\mathbf{q}|))]\ , \end{aligned} \tag{14}$$

with $s_k \equiv \sin\phi_k$, $c_k \equiv \cos\phi_k$ and $x = \hat{\mathbf{k}}\cdot\hat{\mathbf{q}}$. The transversality operator, $\left(\delta_{ij} - \nabla_i\nabla_j/\nabla^2\right)_{\mathbf{x}}$, in the hyperfine interaction generates an additional kernel

$$W(|\mathbf{k}-\mathbf{q}|) \equiv U(|\mathbf{k}-\mathbf{q}|)\frac{x(k^2+q^2) - qk(1+x^2)}{|\mathbf{k}-\mathbf{q}|^2}\ . \tag{15}$$

The meson states were calculated using both the TDA and RPA, the latter being essential to preserve chiral symmetry. The TDA and RPA states are respectively $|\Psi^{nJPC}_{TDA}\rangle = Q^\dagger_{nJPC}(TDA)|\Omega\rangle$, $|\Psi^{nJPC}_{RPA}\rangle = Q^\dagger_{nJPC}(RPA)|\Omega_{RPA}\rangle$, with radial-node quantum number n. The two meson operators are

$$Q^\dagger_{nJPC}(TDA) = \sum_{c\mu\overline{\mu}}\int \frac{\mathrm{d}\mathbf{k}}{(\mathbf{2}\pi)^{\mathbf{3}}}\Psi^{nJPC}_{\mu\overline{\mu}}(\mathbf{k})B^{c\dagger}_\mu(\mathbf{k})D^{c\dagger}_{\overline{\mu}}(-\mathbf{k})\,, \tag{16}$$

$$Q^\dagger_{nJPC}(RPA) = \sum_{c\mu\overline{\mu}}\int \frac{\mathrm{d}\mathbf{k}}{(2\pi)^3}[X^{nJPC}_{\mu\overline{\mu}}B^{c\dagger}_\mu(\mathbf{k})D^{c\dagger}_{\overline{\mu}}(-\mathbf{k}) - Y^{nJPC}_{\mu\overline{\mu}}B^c_\mu(\mathbf{k})D^c_{\overline{\mu}}(-\mathbf{k})]\,.$$

The TDA and coupled RPA equations are given in Refs. [1] and [2]. For the vector mesons ρ, J/ψ, the wavefunctions have been generalized to include both s and d waves leading to four coupled RPA equations. The detailed form of the kernels and equations is specified in Ref. [9].

TABLE 1. Hyperfine effective interactions.

Model	Parameters
1. square well	$U_h = \text{GeV}^{-2}$, $\Lambda = 3m_g = 1.95$ GeV
2. Coulomb	$m_g = 0.47$ GeV
3. modified Coulomb	$m_g = 0.65$ GeV
4. Yukawa	$m_g = 0.6$ GeV

TABLE 2. Calculated masses, condensates and data in MeV.

Quantity	Model 1	Model 2	Model 3	Model 4	Experiment
$^\dagger m_u = m_d$	1	1	1	1	1.5-8.5
$^\dagger m_c$	730	675	675	675	1000-1400
$\mathcal{M}_u = \mathcal{M}_d$	104	191	124	125	200-300
$\mathcal{M}_c$	1370	1512	1408	1420	1500
$- < \bar{q}q >^{1/3}$	150	206	165	177	236
M_π	165	129	158	150	138
$M_{\pi(1300)}$	1298	1149	1322	1243	1300
$M_{\pi(1800)}$	1949	1628	2019	1884	1801
M_ρ	714	751	740	712	771
$M_{\rho(1450)}$	1348	1151	1384	1304	1465
$M_{\rho(1700)}$	1554	1292	1564	1493	1700
$M_{\eta_c(1S)}$	2972	2980	2990	2978	2980
$M_{\eta_c(2S)}$	3572	3425	3604	3541	3594
$M_{\eta_c(3S)}$	4031	3708	4034	3929	?
$M_{J/\psi(1S)}$	3090	3146	3117	3109	3097
$M_{\psi(2S)}$	3653	3462	3651	3586	3686
$M_{\psi(3770)}$	3679	3483	3665	3600	3770

†adjusted

Table 1 lists the different interactions and parameters while Table 2 summarizes the current quark masses for the u/d and c flavors and the calculated constitutent quark masses and condensates. The pseudoscalar and vector RPA masses,

along with two radial excited states, are given in Table 2. The hyperfine potential parameters were adjusted to fit the charmonium ground state splittings since chiral symmetry does not effect this system. However, in achieving the desired $\eta_c - \mathrm{J}/\psi$ 120 MeV mass difference, the constituent charmed quark mass also appreciably increased which in turn required a significantly smaller, 675 MeV, charm current mass to reproduce the observed charmonium spectra. This surprising result is due to the Ward identity governing the interaction in the gap equation which generates a much larger self-energy from the hyperfine potential. Then with all interactions fixed, the remaining meson masses were predicted although it was again necessary to reduce the degenerate u/d current quark mass to 1 MeV to obtain a reasonable π mass.

It is significant that this approach is able to simultaneously describe the small charmonium and large π-ρ splittings with the same hyperfine interaction. This is possible because the RPA meson operator commutes with the chiral charge and preserves chiral symmetry yielding a light Goldstone pion. Indeed, the TDA pion for the same $H_{\rm eff}$ has mass about 500 MeV. Hence chiral symmetry is predominantly responsible for the large $\pi - \rho$ splitting, contributing about 400 MeV. Note that the model also describes the excited state spin splittings, typically less than 200 MeV, which are entirely from the hyperfine interaction. These states are not governed by chiral symmetry and the TDA and RPA results agree to within a few percent. Finally, the hyperfine interaction yields an improved condensate between $-(150\,\mathrm{MeV})^3$ and $-(206\,\mathrm{MeV})^3$. The previous result [2] without a hyperfine potential was too small, $\langle\bar{q}q\rangle = -(110\,\mathrm{MeV})^3$.

5. *Summary*

The many-body effective Hamiltonian approach provides a unified quark-gluon framework for realistically describing both glueballs and mesons. The glueball Regge trajectories are in good agreement with the traditional pomeron and recently discovered odd signature daughter. This suggests a strong pomeron-glueball connection which in turn permits predicting glueball production and decay rates and a novel multi-pion detection signature. The same $H_{\rm eff}$, supplemented with a hyperfine interaction, also produces light and heavy meson spin-splitting spectra in good agreement with observation. The model quark, and especially gluon, condensates are also in reasonable agreement with known results, however, this now requires much smaller current quark masses which is a topic for further study.

Acknowledgements

F. J. Llanes-Estrada, A. P. Szczepaniak and R. A. Williams are gratefully acknowledged. Thanks to the NAPP2003@DUBROVNIK Conference organizers, especially B. Vlahovic and I. Supek. Support is from U. S. DOE grant DE-FG02-97ER41048.

References

[1] F. J. Llanes-Estrada and S. R. Cotanch, Phys. Rev. Lett. **84** (2000) 1102.

[2] F. J. Llanes-Estrada and S. R. Cotanch, Nucl. Phys. A **697** (2002) 303.

[3] A. P. Szczepaniak et al., Phys. Rev. Lett. **76** (1996) 2011.

[4] F. J. Llanes-Estrada et al., Nucl. Phys. A **710** (2002) 45.

[5] F. J. Llanes-Estrada and S. R. Cotanch, Phys. Lett. B **504** (2001) 15.

[6] N. I. Kochelev et al., Phys. Rev. D **67** (2003) 074014.

[7] C. J. Morningstar and M. Peardon, Phys. Rev. D **60** (1999) 034509; G. S. Bali et al., Phys. Lett. B **309** (1993) 378; H. Chen et al., Nucl. Phys. B **34** (1994) 357; M. Teper, hep-th/9812187 (1998); D. Q. Liu and J. M. Wu, hep-lat/0105019 (2002).

[8] H. B. Meyer and M. Teper, hep-lat/0306019 (2003); hep-lat/0308035 (2004).

[9] F. J. Llanes-Estada, S. R. Cotanch, A. P. Szczepaniak and E. S. Swanson, in press Phys. Rev. C.

[10] A. P. Szczepaniak and E. S. Swanson, Phys. Rev. D **62** (2000) 094027.

COULOMBOV BAŽDARNI HAMILTONIJAN: NAPREDAK I PRIMJENE

Daje se pregled teorijskog razvoja i primjena efektivnog Hamiltonijana QCD u Coulombskoj baždarnosti. Navode se višečestične BCS, TDA i RPA dijagonalizacije u kvarkovskom i gluonskom sektoru za spektre mezona i gluonskih lopti. Reggeove putanje modelskih gluonskih lopti su u dobrom skladu s potvrđenim pomeronom i nedavno opaženom kćeri s neparnim znakom. Primjenom veze pomeron – gluonska lopta i prevladavanja vektorskih mezona, izračunali smo udarne presjeke za fototvorbu gluonskih lopti i njihovih raspada, i predviđaju se značajke za eksperimentalno nalaženje. Također se istražuju cijepanja masa pseudoskalarno-vektorskih mezona zasnovana na poprečnoj izmjeni gluona. Postigli smo poboljšan spektar mezona i potvrdili prevladavajuću ulogu kiralne simetrije glede razlike masa π i ρ.